Article

Applied Spectroscopy

www.s-a-s.org

Applied Spectroscopy
0(0) 1–10

DOI: 10.1177/0003702817732324
journals.sagepub.com/home/asp

SAGE

Binary Complementary Filters for Compressive Raman Spectroscopy

Owen G. Rehrauer[1], Vu C. Dinh[2], Bharat R. Mankani[1], Gregery T. Buzzard[3], Bradley J. Lucier[4], and Dor Ben-Amotz[1]

Abstract

The previously described optimized binary compressive detection (OB-CD) strategy enables fast hyperspectral Raman (and fluorescence) spectroscopic analysis of systems containing two or more chemical components. However, each OB-CD filter collects only a fraction of the scattered photons and the remainder of the photons are lost. Here, we present a refinement of OB-CD, the OB-CD2 strategy, in which all of the collected Raman photons are detected using a pair of complementary binary optical filters that direct photons of different colors to two photon counting detectors. The OB-CD2 filters are generated using a new optimization algorithm described in this work and implemented using a holographic volume diffraction grating and a digital micromirror device (DMD) whose mirrors are programed to selectively direct photons of different colors either to one or the other photon-counting detector. When applied to pairs of pure liquids or two-component solid powder mixtures, the resulting OB-CD2 strategy is shown to more accurately estimate Raman scattering rates of each chemical component, when compared to the original OB-CD, thus facilitating chemical classification at speeds as fast as 3 μs per measurement and the collection of Raman images in under a second.

Keywords

Raman spectroscopy, chemometrics, compressive sampling

Date received: 9 May 2017; accepted: 4 July 2017

Introduction

Raman spectroscopy takes advantage of the inelastic scattering of light by molecular vibrational modes. The resulting Raman spectrum provides a fingerprint which can be used for chemical classification (identification), quantitation, and chemical imaging measurements, in a wide variety of implementations and applications.[1,2] However, the low probability of spontaneous Raman scattering events means that it often requires about 1 s (or longer) to obtain a single high-quality Raman spectrum from a liquid or solid sample. Thus, conventional Raman spectral measurement strategies are far too slow to be compatible with real-time chemical imaging and high-speed chemical kinetics applications that require millisecond (or microsecond) time resolution (per measurement or per hyperspectral image pixel).

The speeds at which Raman spectral information may be obtained can be increased by using compressive hyperspectral detection strategies, in which either a liquid-crystal tunable-filter (LCT)[3–7] or digital micro-mirror device (DMD)[8–13] is used to multiplex photons of different selected wavelengths onto a single-channel detector.This is advantageous because of the fast read times and low noise of single-channel photon-counting detectors when compared to multichannel detectors such as a charge-coupled device (CCD) detector array. Most importantly, multiplexing light from multiple wavelengths onto a single photon-counting detector produces far less read and dark noise than would have been obtained if the same photons were distributed onto multiple CCD pixels.[6,13,14]

Here we present a significant extension of the previously described DMD-based optimized binary compressive detection (OB-CD) strategy.[13–16] This new strategy (OB-CD2) uses two detectors to count all of the collected photons transmitted by two complementary binary optical

[1]Department of Chemistry, Purdue University, West Lafayette, IN, USA
[2]Program in Computational Biology, Fred Hutchinson Cancer Research Center, 1100 Fairview Avenue North, Seattle, WA, USA
[3]Department of Mathematics, Purdue University, West Lafayette, IN, USA
[4]Department of Mathematics and Department of Computer Science, Purdue University, West Lafayette, IN, USA

Corresponding author:
Dor Ben-Amotz, Department of Chemistry, Purdue University, West Lafayette, IN, USA.
Email: bendor@purdue.edu

filters. Thus OB-CD2 has some similarity to the recently described LCT-based multivariate optical computing strategy,[7] as both methods are able to simultaneously classify more than one chemical component. Our results demonstrate faster chemical classification and hyperspectral imaging speeds obtainable using OB-CD2 compared to OB-CD. We have previously demonstrated that the OB-CD chemical classification performance obtainable using binary (i.e., DMD-based) filters is essentially equivalent to that theoretically obtainable using analogue (i.e., LCT-based) filters.[13] We have also previously demonstrated the use of OB-CD for high-speed chemical imaging and three component concentration measurements,[14] as well as for quantitation in the presence of fluorescence interference and photobleaching.[16]

The remainder of this manuscript is organized as follows. In the Experimental and Theoretical Methods section, we describe the newly derived algorithm used to generate OB-CD2 filters, designed to efficiently distinguish two or more components based on differences in their Raman spectra. The "Experimental and Theoretical Methods" section and subsection entitled "OB-CD2 Spectrometer" describes the optical system used to perform both OB-CD and OB-CD2 measurements, and the materials used to quantitatively compare OB-CD and OB-CD2 chemical classification and imaging performance. The section "Results and Discussion" describes results obtained using samples with between two and four spectrally distinct chemical components, including both liquid classification and solid chemical imaging. The "Conclusion" section includes a discussion of the key differences and unique capabilities of the OB-CD and OB-CD2 strategies.

Experimental and Theoretical Methods

Binary-Complementary Filter Generation

OB-CD2 is a derivative of OB-CD and, as a result, many of the assumptions made in OB-CD filter generation hold true for OB-CD2. The theorems and resulting algorithms used to generate OB-CD filters have previously been described,[13,15] as have the chemical imaging and quantitation performance obtainable using OB-CD.[14,16] Here, we highlight differences between OB-CD and OB-CD2, and briefly summarize common features and assumptions made in implementing both OB-CD and OB-CD2. Most importantly, OB-CD uses binary optical filters, each of which multiplexes and directs light in selected wavelength channels onto one photon-counting detector and discards the remainder, while OB-CD2 uses a two-detector system with filters that direct some selected photons to one detector and the remainder to another detector. Moreover, while the OB-CD filter generation algorithm minimizes the sum of the variances of the estimated Raman scattering rates of all chemical components, the OB-CD2 algorithm minimizes the total volume of the multidimensional ellipsoidal confidence regions derived from the covariance matrix of the estimated Raman scattering rates.

We let *P* be a matrix with *n* columns of length *N*, each containing the area-normalized spectrum of some known chemical component divided into *N* energy bins, and Λ be a (column) *n*-vector of mean photon emission rates of each of the chemical components under consideration. While the variance of our estimators will depend on the true (unknown) mean photon emission rates Λ, we design our algorithm to minimize that variance for a particular vector of rates $\bar{\Lambda}$ (obtained as further discussed below). In our experience, a mismatch between Λ and $\bar{\Lambda}$ has little effect on the filters constructed or the variance of the estimated rates.

We assume that independent measurements of either pure components or mixtures are made and that in the *k*th measurement, the probability that a photon with energy falling in the *i*th bin will be counted is given by F_{ik}, the *ik*-entry of the matrix of filters *F* (so, $0 \leq F_{ik} \leq 1$). The *k*th column of *F* is referred to as the *filter* for the *k*th measurement.

As with OB-CD, given the vector $\hat{x}$ containing the empirical photon counts transmitted through each filter in *F*, we estimate the true photon emission rates Λ using the unbiased estimator $\hat{\Lambda} = B\tau^{-1}T^{-1}\hat{x}$, where *T* is a matrix whose diagonal elements indicate the fraction of the total measurement time, τ, that each filter in *F* is applied, and *B* is a left inverse of F^TP, i.e., $BF^TP = I_{n\times n}$ (where $I_{n\times n}$ is an identity matrix). If $m = n$, i.e., we take the same number of measurements as there are chemical species, then $B = (F^TP)^{-1}$.

The objective of OB-CD2 is to construct a matrix of filters of a special form that minimizes the determinant of the variance-covariance matrix of $\hat{\Lambda}$ if we assume that $\Lambda = \bar{\Lambda}$:

$$Q(B, T, F, \bar{\Lambda}) = \det\left[\tau^{-1}BT^{-1}\mathrm{diag}\left(TF^TP\bar{\Lambda}\right)T^{-1}B^T\right] \quad (1)$$

We constrain *F* to consist of pairs of binary-complementary filters, that is, each entry in F_{ij} is either 0 or 1, and the set of filters are collected into pairs each of which sum to a vector of all ones. Minimizing the determinant for OB-CD2 corresponds to the *D*-optimality criteria of experimental design, in contrast to the *A*-optimality criteria considered in the setting of OB-CD, which minimizes the sum of the variances of the estimators $\hat{\Lambda}_i$. Again, *A*-optimality chooses filters that minimize the sum of the variances of the $\hat{\Lambda}_i$, *D*-optimality chooses filters that minimize the volume of the confidence ellipsoids for $\hat{\Lambda}$. For more discussion of *D*-optimality and *A*-optimality criteria, see, for example, Atkinson et al.[17] and Pukelsheim.[18]

In our previous implementations of OB-CD, we generally used the same number of measurements/filters (*m*) as chemical species (*n*). For OB-CD2, we build $m = n - 1$

pairs of complementary filters (that is, 2 *m* filters in total). These are the minimum number of filters needed by each of OB-CD and OB-CD2 to estimate emission rates for *n* chemical species.

The construction of the OB-CD2 optimal filter design is supported by the following observations. First, we note that, as with OB-CD, the value of *Q* obtained by taking $\bar{\Lambda} = \Lambda_0$, the vector of the form $(1, \ldots, 1)^T$ of length *n*, provides reasonable filters for any practical value of Λ. Second, while optimizing *Q* over all variables is difficult, this problem can be solved efficiently when certain dependencies between the variables are imposed. Specifically, for fixed values of *T* and $A = F^{TP}$, the unique optimal design matrix *B* is given by $B = (A^T T D^{-1} T A)^{-1}\ A^T T D^{-1} T$ where $D = \mathrm{diag}(TA\Lambda_0)$. Similarly, for a fixed value of *F*, if *B* depends on *A* and *T* as described above, then the unique normalized time matrix T^* satisfies $T^*_{kk} = (1/n)[AB]_{kk}$.

This enables us to propose the following procedure to construct the optimal filter design and implement it in Matlab. For a fixed matrix of filters *F*, characterized by *m* base filters and *m* corresponding complementary filters, we compute the optimal normalized time matrix T_F and design matrix B_F as follows.

We write $A = F^T P$, $k' = k + m$ for $k = 1, \ldots, m$, and $\Lambda_0 = (1, \ldots, 1)^T$ of length *n*. We assume that the sum of the *k*th and k'th columns of *F* is a vector of all ones. We start with the initial guess $T_0 = \mathrm{diag}(1/n)$. For $i = 0, 1, \ldots$, we compute

$$B_i = (A^T T_i D_i^{-1} T_i A)^{-1} A^T T_i D_i^{-1} T_i \tag{2}$$

where $D_i = \mathrm{diag}(T_i A \Lambda_0)$, and

$$[T_{i+1}]_{kk} = [T_{i+1}]_{k'k'} = \frac{1}{2}\left([AB_i]_{kk} + [AB_i]_{k'k'}\right) \tag{3}$$

The values of T_{i+1} are then normalized to ensure that the sum of its diagonal components is equal to 1. This iteration is performed 100 times to obtain T_F and B_F. While we have no proof that this iteration converges, it does so for all the examples we have considered.

Finally, the function $Q(B_F, T_F, F, \Lambda_0)$ is then optimized over all possible values of the matrix of filters *F*. This is done by using an algorithm similar to the one used in OB-CD, which combines a linear programming step with a nonlinear optimization step. This algorithm allows the optimal matrix of filters F^* to admit non-binary values. As with OB-CD, the optimal non-binary matrix of filters is nearly binary, in the sense that few entries of F^* are strictly between 0 and 1. A correction step is then performed to produce the optimal binary matrix of filters F^* (as with OB-CD, this consists of rounding non-binary values to 0 or 1), and a final iteration of B_i and T_i computes the corresponding optimal normalized time matrix T^* and design matrix B^*.

OB-CD2 Spectrometer

The schematic of the system used to perform OB-CD2 measurements is shown in Fig. 1. This system was custom-built in collaboration with Laser Labs LLC (Buffalo Groves, USA). This spectrometer will be described in more detail in a forthcoming paper.

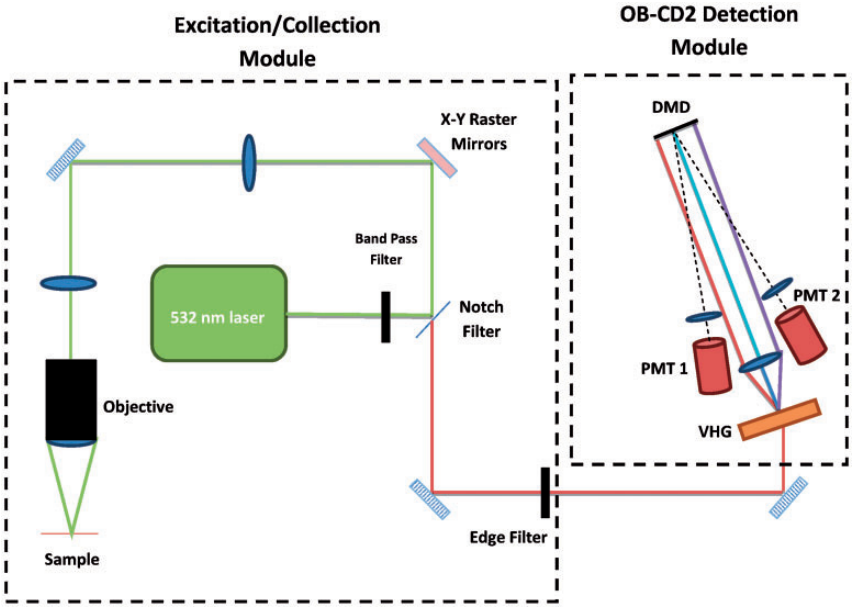

Figure 1. Schematic of the OB-CD2 Raman system with a 532 nm excitation laser.

As with the previously described OB-CD systems,[16] our microscope is configured to collect the backscattered Raman signal with the same objective lens that is used to focus the excitation laser onto the sample. The present system incorporates a 532 nm excitation laser beam (Sapphire SD 532–150 CDRH Laser, with a maximum power of 150 mW), which passes through a laser-line band-pass filer (Semrock RazorEdge LWP Filter, U–grade-25 mm) before it is focused onto the sample using a microscope objective (Olympus MPlan, 20 $\times$, 0.4 NA). The samples are placed on a computer-controlled microscope stage (Prior ProScan III with H31XYZE-US control module). However, all the imaging measurements described in this work (including the video in the online Supplemental Material) were performed by using two galvanometer mirrors to raster scan the light over the sample using an optical design schematically illustrated on the left-hand-side of Fig. 1, with a two-mirror raster scanner and pair lenses to assure that the excitation laser beam remains approximately centered on the objective throughout the raster-scanning process.

The backscattered Raman photons are collected and then transmitted through a dichroic mirror and then through a long pass (edge) filter to reject laser Rayleigh scattering. A volume holographic grating (Wasatch Photonics, $\sim$600 lines mm^{-1}) is used to separate photons of different wavelengths and a lens is used to focus the spectrally dispersed photons onto the DMD surface (Texas Instruments, DLP3000, 608 $\times$ 684 mirror array with 10.8 μm mirror pitch). The spectral window in this system is $\sim$200–4100 cm^{-1}. Pairs of adjacent columns of DMD mirrors are grouped together, yielding a total of 342 different wavelength "bins", each corresponding to a Raman vibrational frequency width of $\sim$12 cm^{-1}. Light reflected by the DMD mirrors is focused onto one of two photon-counting photomultiplier tubes (PMT) modules (Hamamatsu model #H10682-01), which have a dark count rate of $\sim$500 photons s^{-1}. The entire area of the DMD surface is imaged onto the active area of the PMT detector. The TTL output pulses from the PMT module are counted using a USB data acquisition (DAQ) card (National Instruments, USB-6212BNC). The system is controlled using interface software written in Labview 2013. OB-CD2 filter generation is performed as described in the "Binary Complementary Filter Generation", sub-section using a script written in Matlab (v.8.03 R2014a). This system is used to both collect full Raman spectra by programming the DMD mirror to perform either notch scans[13] or spectral Hadamard scans.[19] Similar to other authors,[20] we applied rows of a Hadamard matrix sequentially on the DMD to perform Hadamard scanning. As stated above, each energy bin corresponded to two columns on the DMD. Since it was not possible to construct a 342 $\times$ 342 Hadamard matrix, a 320 $\times$ 320 matrix was used. As a result, the first 22 rows of the DMD were assumed to have zero intensity. Each row in the Hadamard matrix was then turned into two different images, a "positive" image where energy bins corresponding to a value of "1" in the Hadamard matrix were measured at the detector (and applied to all rows of the DMD) and a separate "negative" image where energy bins corresponding to a value of "-1" were measured at the detector. The difference between the counts through the "positive" and "negative" images were calculated to determine the number of counts collected through each row of the Hadamard matrix. An inverse-Hadamard transform was performed to recover a spectrum.

Chemicals Used to Demonstrate Performance

Acetone was acquired from Fischer (HPLC grade, 99.8% purity, batch #0000070736). Benzene was purchased from OmniSolv (99.93% purity, lot #42282). Hexanes were acquired from Baxter (HPLC Grade, 0.001% water, lot #901141). Methylcyclohexane was acquired from Mallinckroft (Anhydrous, 99+% purity, lot #1906 KCBN). Benzoic acid (ACS Reagant Grade, 99.5% purity, lot #26115MA) and acetaminophen (98.0–101.05% purity, lot #SLBC6391V) were obtained from Sigma. The benzoic acid used in this work was heated in acetonitrile and then cooled for 1 h followed by overnight drying to produce large crystals and to remove fluorescent impurities.

Results and Discussion

Comparison of OB-CD and OB-CD2 for Binary Classifications

In previous work,[13] acetone and benzene were classified using OB-CD filters with total integration times as low as 30 μs using a 785 nm excitation laser with 85 mW of power at the sample. Here, we demonstrate the classification of acetone and benzene in 3 μs using a 532 nm excitation laser with 65 mW of laser power at this sample (as further described in subsection "*OB-CD2 Spectrometer*"), using both the OB-CD and OB-CD2 filter generation and detection strategies. Figure 2 shows the training spectra (curves), with the resulting OB-CD (left) and OB-CD2 (right) filters (shaded regions) overlaid on the spectra. The bottom portion of Fig. 2 shows the resulting Raman scattering rate estimates for pure acetone (on the horizontal axis) and pure benzene (on the vertical axis) obtained using a total integration of time of 3 μs. Note that the resulting 95% confidence interval ellipses for acetone and benzene overlap in the case of the OB-CD recovered rates, but do not overlap in the case of the OB-CD2 recovered rates. This demonstrates that, at a fixed total integration time, Raman scattering rates recovered using OB-CD2 filters have lower variance than the Raman scattering rates recovered using OB-CD filters. The lower variance obtained using OB-CD2

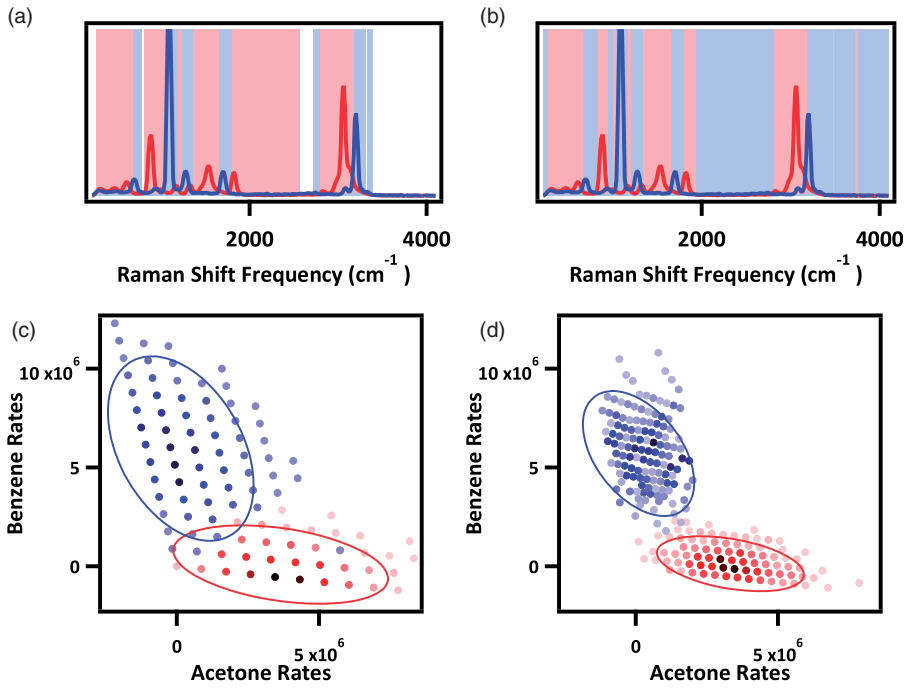

Figure 2. Comparison of the spectra, filters, and recovered Raman scattering rates of acetone (red) and benzene (blue) obtained using OB-CD and OB-CD2 with total integration time of 3 μs per measurement. The shaded regions in (a) OB-CD and (b) OB-CD2 indicate the wavelengths transmitted to the corresponding binary optical filters, and the curves represent the Raman spectra of the two components. Scatter plots of the acetone and benzene recovered Raman scattering rates are shown in (c) OB-CD and (d) OB-CD2. The darkness of each colored point represents the number of times out of 1000 experiments the corresponding pair of photon rates was obtained; in (c) the lightest and darkest blues represent 1 and 59, respectively, and the lightest and darkest reds represent 1 and 111, respectively; in (d) the lightest and darkest blues represent 1 and 33, respectively, and the lightest and darkest reds represent 1 and 58, respectively. The ellipses in (c) and (d) indicate the 95% confidence intervals of the recovered Raman scattering rates. The percent of the total measurement time for the OB-CD filters was 52% for the filter shown in red and 48% for filter shown in blue. The single OB-CD2 filter pair was applied for 100% of the total measurement time. The points in (d) are closer together than the points in (c) because we capture more photons with OB-CD2 than with OB-CD in a given time, so each additional photon captured by a filter has a smaller influence on the resulting estimated rates.

is linked to the fact that more photons are detected using OB-CD2 than OB-CD. More specifically, on average, OB-CD2 filters lead to the detection of 10.4 (range = 0–20) photons for acetone and 17.4 (range = 0–25) photons for benzene, whereas OB-CD filters lead to the detection of 4.2 (range = 0–11) and 6.9 (range = 0–13) photons, respectively. The OB-CD2 recovered Raman scattering rates of acetone and benzene have a 35% lower total variance than the OB-CD recovered Raman scattering rates.

Comparison of OB-CD and OB-CD2 for Ternary and Quaternary Classifications

Here, we compare the recovered Raman scattering rates estimated using OB-CD and OB-CD2 filters trained to detect three different pure liquids ($n = 3$): benzene, hexane, and methylcyclohexane. These three components are classified using two complementary pairs of OB-CD2 filters since, as noted in subsection "*Binary-Complementary Filter Generation*," OB-CD2 requires a minimum of $2(n-1)$ filters, consisting of $n-1$ pairs of complementary filters, to describe a system with n components. Figure 3a presents a heat map illustrating the relationship between the training spectra and resulting OB-CD filters, with the inner product between each filter vector and each normalized spectral vector represented using a color (as denoted by the color bars). Figure 3b shows the OB-CD2 filters for the same spectral training set; filters 1 and 3, and filters 2 and 4, are complementary. These heat maps illustrate the fact that there is no one-to-one correspondence between each filter and the spectrum of a particular component. Rather, the photon counts detected using all the filters are processed to estimate the rates of each of the chemical components as described in subsection "Binary-Complementary Filter Generation".

Similar OB-CD and OB-CD2 procedures were used to estimate the Raman scattering rates of pure benzene, hexane, and methylcyclohexane with a laser power 25 mW at the sample, and a total integration time of 1 ms. Figure 4 summarizes these results, with panels (a–c) showing projections of the 95% confidence ellipses onto the benzene-hexane, benzene-methylcyclohexane, and hexane-methylcyclohexane

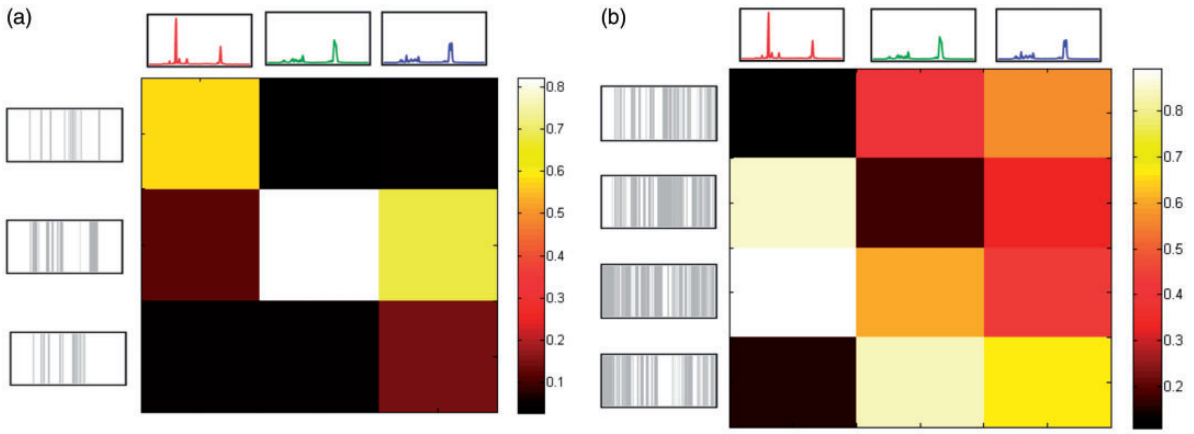

Figure 3. (a) OB-CD and (b) OB-CD2 show the corresponding spectra (rows), filters (columns), and heat maps pertaining to the classification of benzene (red spectrum), hexane (green spectrum), and methylcyclohexane (blue spectrum). The heat map color bars represent the vector dot product of the corresponding spectra and filters; the filters for OB-CD have been ordered so that the diagonal contains the largest overlap values for each filter. The measurement time for each of the OB-CD filters was 16.4%, 22.6%, and 60.9%, respectively, while that for each pair of OB-CD2 filters was 50% of the total time.

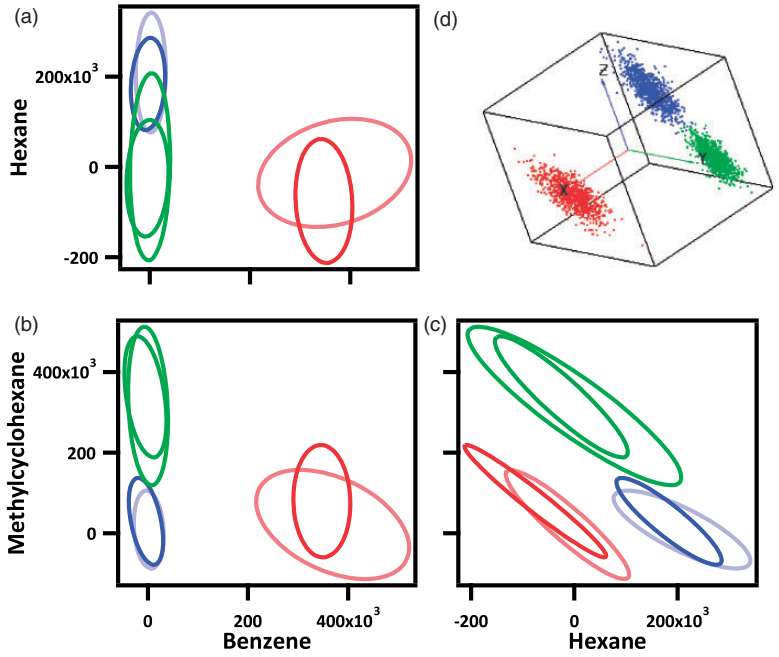

Figure 4. (a–c) The ellipses represent 95% confidence limits of the recovered Raman scattering rates for samples of benzene (red), hexane (blue), and methylcyclohexane (green), obtained using OB-CD (lighter colors) and OB-CD2 (darker colors), with a laser power of 25 mW and an integration time of 1 ms. Each plot shows two-dimensional projections of the three-dimensional classification space. (d) The three-dimensional scatter plot shows all of the OB-CD2 recovered Raman scattering rates, with the *x*-, *y*-, and *z*-axes representing the recovered rates of benzene, hexane, and methylcyclohexane, respectively. The slight bias in the OB-CD2 results (specifically, non-zero mean recovered photon emission rates for chemical components not present in a sample) is due to the fact that the system, as currently configured, does not have precisely the same photon counting efficiency in detectors 1 and 2.

planes, respectively. The points in the cube shown in panel (d) represent OB-CD2 data points from which the results in panels (a–c) were obtained, with each point corresponding to an individual OB-CD2 measurement, and the *x*-, *y*-, and *z*-axes pertaining to benzene, hexane, and methylcyclohexane, respectively.

Table I reports the standard deviations of the estimated recovered Raman scattering rates of for each of the above

components, quantifying the performance advantage of OB-CD2 over OB-CD. The row of Table 1 labeled "Benzene" reports the standard deviations (for OB-CD and OB-CD2) of the estimated benzene Raman scattering rates for a sample of pure benzene, the row labeled "Hexane" reports the estimated hexane Raman scattering rates for a sample of pure hexane, etc. These standard deviations are related to the widths of the ellipses shown in Fig. 4a–c. For example, the large difference in the length in the "Benzene" dimension of the red ellipses in Fig. 4a is reflected in the 62.8% reduction in the standard deviation of the benzene rates. The data in Table 1 demonstrate that, for pure samples, there is less variance in the recovered Raman scattering rates for OB-CD2 when compared to OB-CD. There was a 36% decrease in the average sum of the variances of the recovered Raman scattering rates between OB-CD2 and OB-CD (which corresponds to the volume of the cloud of the data points plotted in Fig. 4d).

Measurements similar to those described above were performed on a four-component system consisting of pure liquid acetone, benzene, hexane, and methylcyclohexane. The resulting spectra, filters, and heat maps are shown in Fig. 5. Note that in this case there are four OB-CD filters and 2(4 – 1) = 6 OB-CD2 filters (or three complementary filter pairs). These measurements were performed with a laser power of 25 mW at the sample and a total integration time of 10 ms for both the OB-CD and the OB-CD2 measurements. Figure 6 shows the resulting 95% confidence ellipses obtained using OB-CD and OB-CD2. Note that, as with the three-component classification, the recovered Raman scattering rate ellipses are invariably smaller for OB-CD2 than OB-CD. The corresponding standard deviations of the estimated recovered Raman scattering rates are reported in Table 2 (in the same way as the three-component results in Table 1). These results indicate that, in comparison with OB-CD, OB-CD2 again produces a 32% decrease in the average sum of the variances of the recovered Raman scattering rates.

Table 1. Standard deviation of recovered Raman scattering rates for ternary classifications.

Sample	OB-CD (counts/s)	OB-CD2 (counts/s)	Decrease (%)
Benzene	6.24×10^4	2.32×10^4	62.8
Hexane	5.41×10^4	4.17×10^4	22.9
Methylcyclohexane	8.03×10^4	6.14×10^4	23.5

Fast Raman Imaging Using OB-CD2

Here, we demonstrate the utility of OB-CD2 as a means of real-time chemical imaging, using a two-component model pharmaceutical composite sample. The sample was produced by using a spatula to gently crush and grind large benzoic acid and acetaminophen crystals to micro-crystalline powders. Small piles of the resulting powers were placed on a gold microscope slide and flattened. The following results were obtained by imaging a region at the interface between the two different types of crystals.

Training was performed using six spectra obtained from different locations in each of the two pure microcrystalline powders. The average, rather than any one of the individual measured spectra, were used for training, as small differences were observed in the relative intensity of Raman

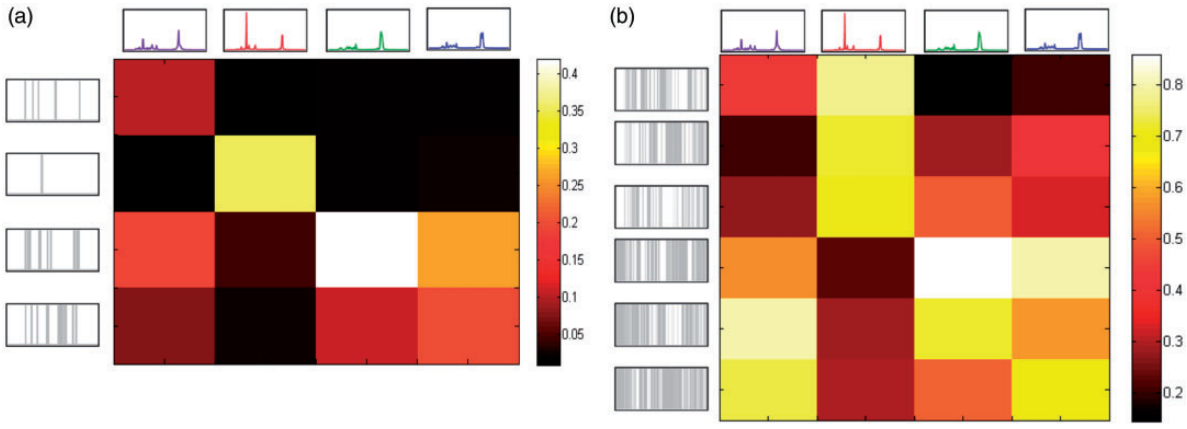

Figure 5. (a) OB-CD and (b) OB-CD2 show the corresponding spectra (rows), filters (columns), and heat maps pertaining to the classification of acetone (purple spectrum), benzene (red spectrum), hexane (green spectrum), and methylcyclohexane (blue spectrum). The heat map is constructed as described in Fig. 3. The heat map color bars represent the vector dot product of the corresponding spectra and filters; for OB-CD the filters have been ordered so that the diagonal contains the largest overlap values for each filter. The measurement time for each of the OB-CD filters was 28.0%, 11.4%, 24.9%, and 35.7%, while that for each pair of OB-CD2 filters was ~33.3% of the total time. Filters 1 and 4, 2 and 5, and 3 and 6 are complementary.

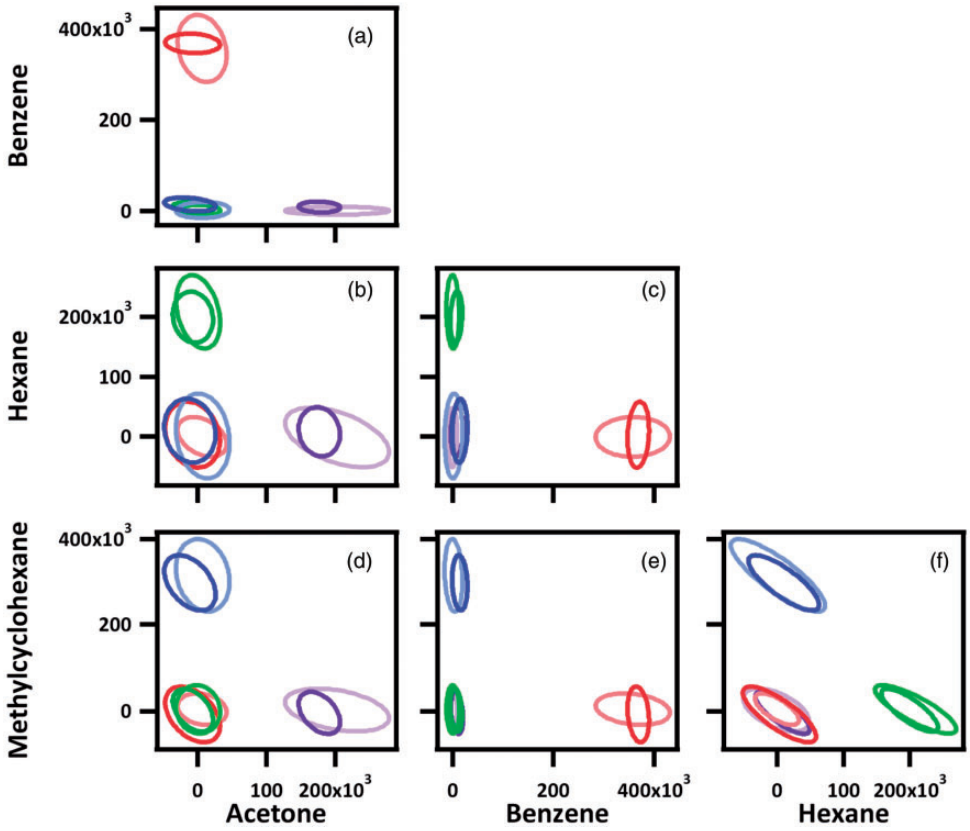

Figure 6. (a–f) 95% confidence ellipses pertaining to the Raman scattering rates of each component, obtained using OB-CD (lighter colors) and OB-CD2 (darker colors), for acetone (purple), benzene (red), hexane (blue), and methylcyclohexane (green), obtained using a laser power of 25 mW and total measurement time of 10 ms. Each plot shows a two-dimensional projection of the four-dimensional recovered Raman scattering rate space, as in Fig. 4.

Table 2. Standard deviation of recovered Raman scattering rates for quaternary classifications.

Sample	OB-CD (counts/s)	OB-CD2 (counts/s)	Decrease (%)
Acetone	3.09×10^4	1.23×10^4	60.2
Benzene	3.01×10^4	0.88×10^4	70.1
Hexane	2.51×10^4	1.74×10^4	30.6
Methylcyclohexane	3.41×10^4	2.52×10^4	26.1

peaks taken at different points on the surface of pure acetaminophen and benzoic acid. These differences are attributed to differences in crystal orientation. We have found that the orientationally averaged spectra of such anisotropic crystal samples provide robust training spectra for subsequent generation of OB-CD and OB-CD2 filters. The resulting OB-CD2 filters for acetaminophen and benzoic acid are shown in Fig. 7a.

Once OB-CD2 filters were trained, a $600 \times 600\,\mu m$ area, consisting of 240×240 pixels, at the interface between acetaminophen and benzoic acid was imaged using a $20\times$ microscope objective at varying integration times. Figure 7b and c show two of these images, taken at integration times of 100 μs/pixel and 10 μs/pixel. Note that 40 pixels at the top and left of these images have been truncated in order to minimize a "blurring" resulting from a hysteresis in the raster scanning mirrors when moving at high speeds. Including these pixels in the integration times gives a total image time of 5.76 s and 0.576 s, respectively (corresponding to frame rates of 0.17 and 1.7 frames/s, respectively. However, neglecting the dead time associated with measuring these pixels and only accounting for the measurement of the 200×200 pixel images shown in Fig. 7b and c yields measurement times of 4 s and 0.4 s per frame.

Additionally, a movie was made using these OB-CD2 filters with a frame rate of 0.576 s (10 μs/pixel). The benzoic acid and acetaminophen crystals were mixed together and placed on a gold microscope slide. Then, the computer-controlled microscope stage was programmed to move to four different positions, each approximately 1 mm apart in a square pattern, which corresponded to four different regions over the surface of the benzoic acid/acetaminophen crystals. The stage was programmed to spend

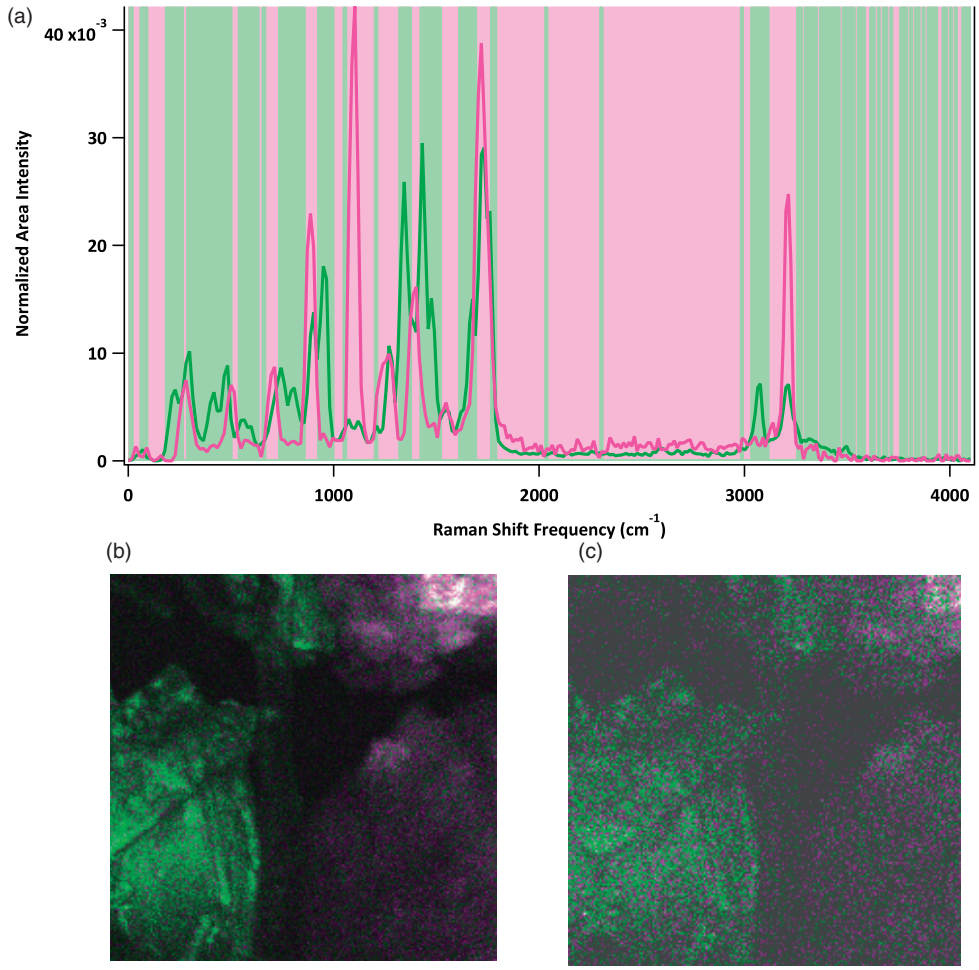

Figure 7. (a) OB-CD2 filters generated for acetaminophen and benzoic acid are shown overlaid the area-normalized spectra of acetaminophen (green spectrum) and benzoic acid (magenta spectrum). Each OB-CD2 filter was applied for 100% of the total measurement time. For this work, the laser power at the sample was set to 65 mW. (b, c) Images of the interface of piles of acetaminophen (green) and benzoic acid (magenta) powders taken at (a) 100 μs/pixel and (b) 10 μs/pixel integration time.

2 s at each region before moving to the next, in a loop that revisited each location ten times. The resulting movie is provided in the Supplemental Material. Note that in the movie the benzoic acid signal is colored red and the acetaminophen signal is colored green.

Conclusion

We have extended the OB-CD hyperspectral Raman sensing and imaging strategy to OB-CD2, which incorporates a second photon-counting detector to simultaneously collect photons transmitted through a pair of complementary binary optical filters. Moreover, we have derived a new algorithm for the generation of optimal filters for OB-CD2. This algorithm differs from that previously derived and used for OB-CD measurements.[13–16] Our results demonstrate that OB-CD2 outperforms OB-CD in the classification of up to four components using up to three pairs of complementary OB-CD2 filters. We have further demonstrated the feasibility of collecting chemical images in under 1 s using OB-CD2.

Both OB-CD and OC-CD2 may be used to identify and quantify Raman and/or fluorescence spectra, as previously described.[16] The maximum speed of OB-CD and OB-CD2 is limited by the sample's Raman/fluorescence light intensity and the maximum linear range of the photon-counting detector, which in the present studies is approximately 5 MHz. Obtaining optimal OB-CD and OB-CD2 results requires that the training and test spectra are spectrally registered, as is the case in conventional full spectral library look-up applications.

Although we have shown that OB-CD2 outperforms OB-CD, there are nevertheless some advantages to OB-CD. First of all, OB-CD requires only a single detector and thus may be implemented more simply (and less expensively). A second more subtle potential advantage of

OB-CD over OB-CD2 derives from the fact that OB-CD filters may be constructed in such a way that some wavelength channels are not detected, thus making it possible to mask regions that do not contain useful chemical information. It is not possible to do so using OB-CD2 since all the collected photons are necessarily transmitted by one of the two complementary binary optical filters and thus detected by one of the two detectors. Thus, when using OB-CD2, rejecting photons in particular wavelength channels could be achieved by using either a physical or spectral mask to prevent those photons from being directed toward the OB-CD2 detectors.

The most significant advantage of OB-CD2 over OB-CD is realized when classifying, quantifying, or imaging systems that contain only two significant chemical (spectral) components. In such situations, one can use a single OB-CD2 complementary filter pair to classify/quantify the two components, without incurring any dead-time or delay associated with switching the DMD mirror settings. Thus, two component chemical images can be obtained in a single raster-scan over the area of interest, rather than requiring two image scans using different OB-CD filters (or using an even more time-consuming process of switching between filters at each point in a single scan). This advantage of OB-CD2 over OB-CD not only facilitates high-speed imaging, but should also make it possible to perform chemical kinetic measurements using a single pair of OB-CD2 filters that are trained to recognize the spectral signatures associated with the reactant and product of a chemical reaction.

Conflict of Interest

The authors report there are no conflicts of interest.

Funding

The work was supported in part by the Office of Naval Research (Contract N0001413-0394 to DBA, GTB, and BJL) and the Simons Foundation (Award #209418 to BJL).

Supplemental Material

All supplemental material mentioned in the text, consisting of a video, is available in the online version of the journal.

References

1. L.A. Nafie. "Recent Advances in Linear and Non-linear Raman Spectroscopy. Part IX". J. Raman Spectrosc. 2015. 46(12): 1173–1190.
2. S. Kumar, T. Verma, R. Mukherjee, F. Ariese, et al. "Raman and Infra-Red Microspectroscopy: Towards Quantitative Evaluation for Clinical Research by Ratiometric Analysis". Chem. Soc. Rev. 2016. 45(7): 1879–1900.
3. W.C. Sweatt, C.A. Boye, S.M. Gentry, M.R. Descour, et al. "Isis: An Information-Efficient Spectral Imaging System". SPIE Proceedings. 1998. 3438: 98–106.
4. N. Uzunbajakava, P. de Peinder, G.W. t Hooft, A.T.M. van Gogh. "Low-cost Spectroscopy with a Variable Multivariate Optical Element". Anal. Chem. 2006. 78(20): 7302–7308.
5. D.C. Maltas, K. Kwok, P. Wang, L.S. Taylor, et al. "Rapid Classification of Pharmaceutical Ingredients with Raman Spectroscopy using Compressive Detection Strategy with PLS-DA Multivariate Filters". J. Pharm. Biomed. Anal. 2013. 80: 63–68.
6. B.M. Davis, A.J. Hemphill, D.C. Maltas, M.A. Zipper, et al. "Multivariate Hyperspectral Raman Imaging Using Compressive Detection". Anal. Chem. 2011. 83(13): 5086–5092.
7. J.E. Vornehm, A.J. Dong, R.W. Boyd, Z. Shi. "Multiple-Output Multivariate Optical Computing for Spectrum Recognition". Opt. Express. 2014. 21: 25005–25014.
8. Q.S. Hanley, P.J. Verveer, T.M. Jovin. "Optical Sectioning Fluorescence Spectroscopy in a Programmable Array Microscope". Appl. Spectrosc. 1998. 52(6): 783–789.
9. N.T. Quyen, E. Da Silva, N. Quy Dao, M.D. Jouan. "New Raman Spectrometer Using a Digital Micromirror Device and a Photomultiplier Tube Detector for Rapid On-Line Industrial Analysis. Part I: Description of the Prototype and Preliminary Results". Appl. Spectrosc. 2008. 62(3): 273–278.
10. N.T. Quyen, M.D. Jouan, N. Quy Dao, E. Da Silva, D.A. Phuong. "New Raman Spectrometer Using a Digital Micromirror Device and a Photomultiplier Tube Detector for Rapid On-Line Industrial Analysis. Part II: Choice of Analytical Methods". Appl. Spectrosc. 2008. 62(3): 279–284.
11. O.O. Soyemi, F.G. Haiback, P.J. Gemperline, M.L. Myrick. "Nonlinear Optimization Algorithm for Multivariate Optical Element Design". Appl. Spectrosc. 2002. 56(4): 477–487.
12. M.F. Duarte, M.A. Davenport, D. Tarkhar, J.N. Laska, et al. "Single-Pixel Imaging via Compressive Sampling". IEEE Signal Process. Mag. 1998. 25(2): 83–101.
13. D.S. Wilcox, G.T. Buzzard, B.J. Lucier, P. Wang, et al. "Photon Level Chemical Classification Using Digital Compressive Detection". Anal. Chim. Acta. 2012. 755: 17–27.
14. D.S. Wilcox, G.T. Buzzard, B.J. Lucier, O.G. Rehrauer, et al. "Digital Compressive Chemical Quantitation and Hyperspectral Imaging". The Analyst. 2013. 138(17): 4982–4990.
15. G.T. Buzzard, B.J. Lucier. "Optimal Filters for High-Speed Compressive Detection in Spectroscopy". SPIE Proceedings. 2013. 8657: 865707–865717.
16. O.G. Rehrauer, B. Mankani, G.T. Buzzard, B.J. Lucier, et al. "Fluorescence Modeling for Optimized-Binary Compressive Detection Raman Spectroscopy". Opt. Express. 2015. 23(18): 423935–423951.
17. A. Atkinson, A. Donev, R. Tobias. Optimum Experimental Designs, with SAS. Oxford: Oxford University Press, 2007 Vol. 37.
18. F. Pukelsheim. Optimal Design of Experiments. Chichester: John Wiley and Sons Inc., 1993.
19. A.G. Marshall, M.B. Comisarow. "Fourier and Hadamard Transform Methods in Spectroscopy". Anal. Chem. 1975. 47(4): 491A–504A.
20. R.A. DeVerse, R.M. Hammaker, W.G. Fateley. "Realization of the Hadamard Multiplex Advantage using a Programmable Optical Mask in a Dispersive Flat-Field Near-Infrared Spectrometer". Appl. Spectrosc. 2000. 54(12): 1751–1758.